NDT&E International 148 (2024) 103238

Contents lists available at ScienceDirect

NDT and E International

journal homepage: www.elsevier.com/locate/ndteint

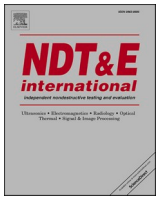

Amplitude-dependent second harmonic Lamb waves for discriminating delamination from background nonlinearities in composite plates

Shengbo Shan [a,b,*], Chi Zhang [a], Gujun Wu [a], Yang Song [c], Ze Liu [c], Yuanman Zhang [c], Li Cheng [c,d,**]

[a] School of Aerospace Engineering and Applied Mechanics, Tongji University, Shanghai, 200092, PR China
[b] Shanghai Institute of Aircraft Mechanics and Control, Shanghai, 200092, PR China
[c] Department of Mechanical Engineering, The Hong Kong Polytechnic University, Kowloon, Hong Kong
[d] Hong Kong Branch of National Rail Transit Electrification and Automation Engineering Technology Research Center, The Hong Kong Polytechnic University, Kowloon, Hong Kong

ARTICLE INFO

Keywords:
Second harmonic Lamb waves
Structural health monitoring
Composites
Delamination
Background nonlinearities

ABSTRACT

Early detection of delamination in composite materials is crucial to maintaining operational safety and reducing excessive maintenance costs. Second harmonic Lamb waves have demonstrated exceptional sensitivity to micro defects in materials including breathing delamination. However, differentiating the second harmonic Lamb waves generated by delamination from other inevitable background nonlinearities, exemplified by inherent material nonlinearity in composites, poses a significant challenge for the practical implementation of the second harmonic Lamb wave-based detection methods. To address this bottle-necking issue, this study examines the characteristics of second harmonic Lamb waves generated by delamination and material nonlinearity, respectively, aiming at their differentiation based on their respective amplitude-dependent features. Results are verified through finite element analysis and experimental validations alongside the verification of the effectiveness of the proposed discrimination strategy. It is shown that the amplitude of the second harmonic waves induced by the delamination is linearly proportional to the fundamental wave amplitude, while the one by the material nonlinearity exhibits a quadratic relationship with the fundamental wave amplitude. Based on this understanding, damage indices are proposed, which prove to be effective for characterizing these two sources of nonlinearity, thereby paving the way for practical delamination detection in composite structures.

1. Introduction

Fiber-reinforced composites have become increasingly prevalent in aerospace, marine, and automotive structures due to their appealing properties such as high specific stiffness, lightweight, customizable characteristics, and resistance to fire and corrosion [1,2]. However, manufacturing defects and accidental damage such as impact damage can compromise the residual strength of these composite structures during service. Accidental impacts, owing to their complex mechanics, can result in barely visible or invisible damage exemplified by delamination between layers [3,4]. Without timely detection, the inter-layer delamination can expand and ultimately lead to catastrophic structural failure. Therefore, the detection and characterization of hidden delamination in composite materials are crucial [5,6].

Guided wave-based structural health monitoring (SHM) techniques have shown promise in detecting concealed defects in multi-layered composite materials [7,8]. These techniques aim at enabling the online and real-time, non-destructive detection and assessment of damage in industrial structural components. By facilitating the estimation of the residual life of structures in service, SHM helps reduce excessive maintenance costs [9,10] and allows for timely decision-making. However, most existing guided wave-based SHM methods rely on linear guided wave scattering phenomena such as reflection, transmission, and mode conversion information at the excitation frequency. Due to the wave-damage interaction mechanisms, the sensitivity of these linear approaches is inherently restricted by the wavelength employed, typically in the millimeter range [11–13].

Recently, the SHM community has increasingly advocated for a ‘shift

* Corresponding author. School of Aerospace Engineering and Applied Mechanics, Tongji University, Shanghai, 200092, PR China.
** Corresponding author. Department of Mechanical Engineering, The Hong Kong Polytechnic University, Kowloon, Hong Kong.
E-mail addresses: shanshengbo@tongji.edu.cn (S. Shan), li.cheng@polyu.edu.hk (L. Cheng).

https://doi.org/10.1016/j.ndteint.2024.103238
Received 26 June 2024; Received in revised form 13 September 2024; Accepted 15 September 2024
Available online 17 September 2024

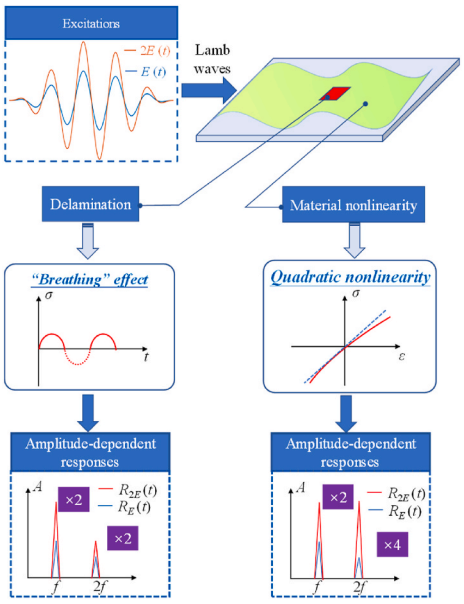

Fig. 1. Amplitude-dependent second harmonic Lamb waves in composite plates.

to the left' maintenance philosophy to achieve early damage detection [5,14–16]. This trend has spurred the advancement of nonlinear guided wave-based techniques for detecting incipient damage in structures. During their propagation, guided waves interact with microstructural defects like lattice anomalies, dislocations, and microcracks to generate various nonlinear wave components. These components include higher harmonics, static component, and mixed frequency components, among others [17–24]. Consequently, nonlinear guided waves exhibit enhanced sensitivity to smaller and invisible damage at the early stage of initiation, a topic that has garnered substantial interest over the past decade.

Second harmonic generation ranks among the most frequently employed weapons for delamination detection [25–31]. The interaction between guided waves and delamination falls within the realm of contact acoustic nonlinearity (CAN) [32–35]. Under the influence of dynamic wave loading, delamination can occasionally manifest as either open or closed, resulting in a phenomenon known as the "breathing effect." This breathing effect is what produces the nonlinear components. While several other mechanisms may also contribute to CAN, including hysteresis, rough surface contact, non-classical dissipation, and more [36], the breathing effect is typically regarded as the predominant cause of the second harmonic generation [24].

The insights mentioned above form the basis for specialized techniques in delamination detection utilizing second harmonic Lamb waves. For instance, Rauter et al. successfully identified impact damage in a unidirectional carbon fiber-epoxy composite by using cumulative second harmonic modes at a specific frequency [37]. Notably, the relative acoustic nonlinearity parameter has shown greater sensitivity to impact damage when compared to the group velocity. In another study, Soleimanpour and Ng detected a carbon fiber-reinforced polymer (CFRP) panel with a transducer array [25]. The temporal information extracted from the second harmonic A0 mode Lamb waves facilitated the identification and localization of embedded delamination in the CFRP panel. Tie et al. conducted extensive numerical and experimental investigations on impact-induced second harmonic Lamb waves, revealing that the relative acoustic nonlinear parameter can escalate with increasing impact energy and delamination areas [38]. More recently, Sikdar et al. introduced a deep learning-based SHM approach for detecting breathing debond in stiffened composite panels [26]. They extracted higher harmonic Lamb wave responses using continuous wavelet transforms and then integrated them into the deep learning framework. The extreme accuracy of the proposed method for multi-level debond detection has been demonstrated.

Despite these successful attempts, the utilization of the second harmonic Lamb waves for practical SHM applications is still in the developmental stage. One major challenge is that the second harmonic Lamb waves generated by delamination are vulnerable to background nonlinearities present in a measurement system. These include instrumentation nonlinearity, transducer nonlinearities, adhesive nonlinearity, and the inherent material nonlinearity of the composites themselves [16,39,40]. Particularly, material nonlinearity is omnipresent and inevitable in composite structures, which naturally interacts with the propagating guided waves to generate second harmonic components [41]. In real-world SHM applications, even if changes in the second harmonic responses are detected, it remains challenging to ensure whether the capture signals are indeed induced by the delamination of interest.

To tackle these challenges, this work systematically investigates the characteristics of the second harmonic Lamb wave generation in composite plates. In particular, amplitude-dependent properties of the second harmonic Lamb waves generated by delamination and material nonlinearity are elucidated and validated through finite element validations. Based on the acquired knowledge, a strategy for the discrimination of delamination-induced second harmonic Lamb waves and those generated by material nonlinearity is proposed. Subsequently, experiments are conducted to validate the theoretically and numerically predicted amplitude-dependent features of the second harmonic Lamb waves and to confirm the efficacy of a proposed strategy for discriminating these two nonlinear sources.

2. Mechanisms of second harmonic Lamb wave generation in composite plates

Considering Lamb waves propagate in a composite plate as sketched in Fig. 1. The second harmonic Lamb waves are generated by different nonlinear sources. The focus of our endeavor is to find ways to separate the second harmonic Lamb waves induced by delamination out of those originating from other alternative sources, deemed as background nonlinearities. The presence of these background nonlinearities would eventually mask the delamination-induced second harmonic Lamb waves. Prominently, the material nonlinearity of the plate is underscored as a representative form of such background nonlinearities.

The nonlinearity arising from the delamination is commonly linked to the CAN. Although CAN involves numerous intricate mechanisms, the most understood one is the "breathing" phenomenon. Should the surfaces at a delaminated section come into contact, any contact pressure can be communicated between them. If this pressure diminishes to zero, the surfaces will diverge. As a result, solely the pressure component of the wave can navigate through the delamination, while the tensile counterpart is inhibited, leading to the manifestation of the second harmonic generation. Given this mechanism, if the amplitude of the incident waves is augmented by a factor of two, it is logically presumed that the response should correspondingly be doubled in the time domain.

Distributed material nonlinearity can also give rise to second harmonic Lamb waves. The elastic behavior of a transversely isotropic material, when quadratic nonlinearity is considered, can be described by the following equation [41]:

$$\mathbf{S}(\mathbf{E}) = 2\alpha_1 \mathrm{tr}(\mathbf{E})\mathbf{I} + \alpha_2(\mathbf{a} \bullet \mathrm{Ea})\mathbf{I} + \alpha_2 \mathrm{tr}(\mathbf{E})(\mathbf{a} \otimes \mathbf{a}) + 2\alpha_3\, \mathbf{E} + 2\alpha_4(\mathbf{a} \bullet \mathrm{Ea})(\mathbf{a} \otimes \mathbf{a}) + \alpha_5(\mathbf{a} \otimes \mathbf{Ea} + \mathbf{aE} \otimes \mathbf{a}) + 3\beta_1(\mathrm{tr}(\mathbf{E}))^2\mathbf{I} + \beta_2 \mathrm{tr}(\mathbf{E}^2)\mathbf{I} + 2\beta_2 \mathrm{tr}(\mathbf{E})\mathbf{E} + \beta_3(\mathbf{a} \bullet \mathrm{Ea})^2\mathbf{I} + 2\beta_3 \mathrm{tr}(\mathbf{E})(\mathbf{a} \bullet \mathrm{Ea})(\mathbf{a} \otimes \mathbf{a}) + \beta_4(\mathbf{a} \bullet \mathbf{E}^2\mathbf{a})\mathbf{I} + \beta_4 \mathrm{tr}(\mathbf{E})(\mathbf{a} \otimes \mathbf{Ea} + \mathbf{aE} \otimes \mathbf{a}) + 2\beta_5 \mathrm{tr}(\mathbf{E})(\mathbf{a} \bullet \mathrm{Ea})\mathbf{I} + \beta_5(\mathrm{tr}(\mathbf{E}))^2(\mathbf{a} \otimes \mathbf{a}) + 2\beta_6 \mathbf{E}(\mathbf{a} \bullet \mathrm{Ea}) + \beta_6 \mathrm{tr}(\mathbf{E}^2)(\mathbf{a} \otimes \mathbf{a}) + 3\beta_7 \mathbf{E}^2 + 3\beta_8(\mathbf{a} \bullet \mathrm{Ea})^2(\mathbf{a} \otimes \mathbf{a}) + \beta_9(\mathbf{a} \bullet \mathbf{E}^2\mathbf{a})(\mathbf{a} \otimes \mathbf{a}) + \beta_9(\mathbf{a} \bullet \mathrm{Ea})(\mathbf{a} \otimes \mathbf{Ea} + \mathbf{aE} \otimes \mathbf{a}) \quad (1)$$

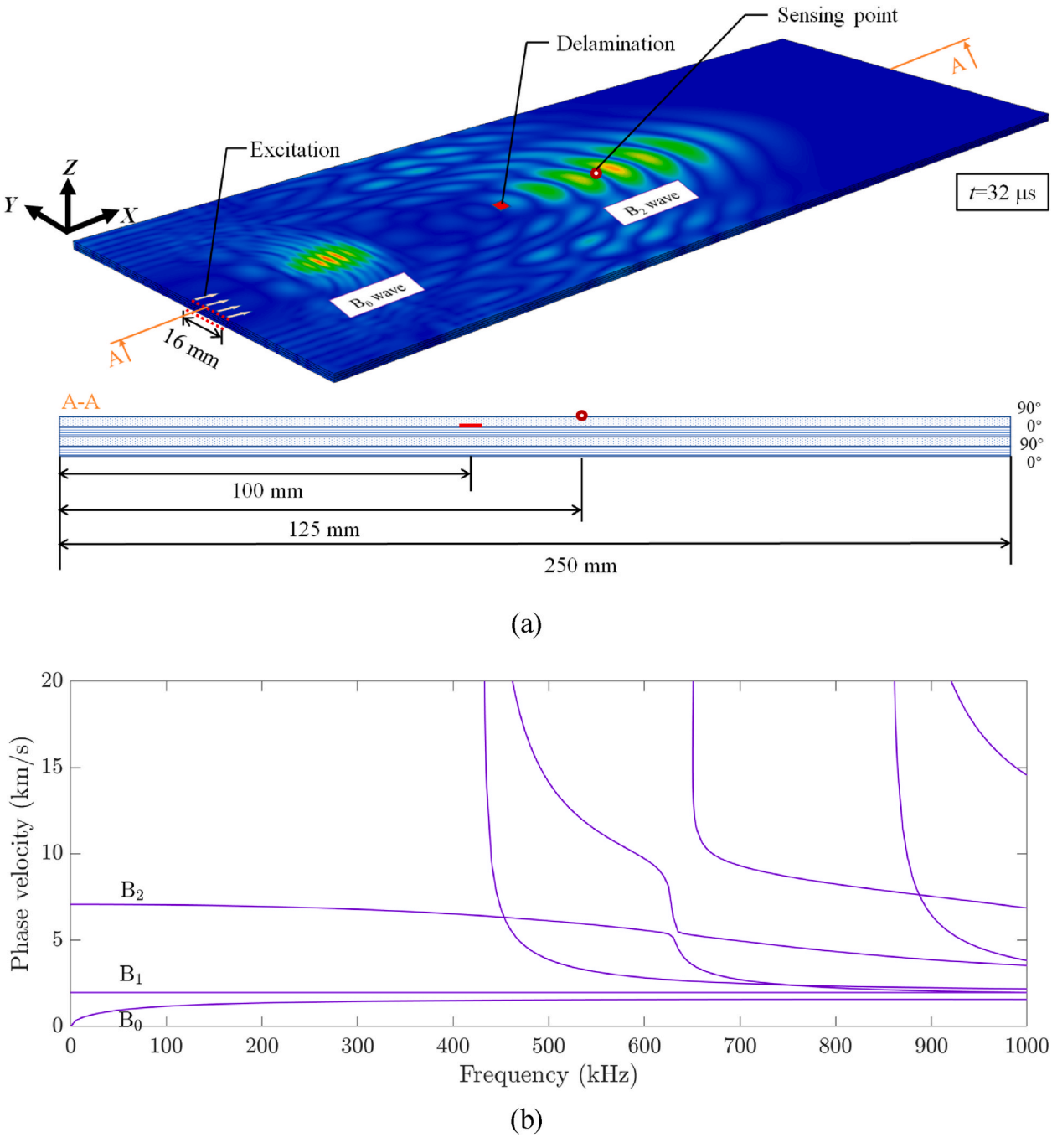

Fig. 2. (a) Sketch of the finite element model; (b) dispersion curves of guided waves propagating at 0° in the $[0°/90°]_2$ composite plate.

where **S** and **E** denote the second Piola-Kirchhoff stress and the Green-Lagrange strain, respectively. The linear and nonlinear elastic coefficients, designated α_i (i = 1,2, …,5) and β_j (j = 1,2, …,9), respectively, are employed in this context. A unit vector **a** is defined as the direction of the material principal axis. The operation tr[] represents the trace of a matrix, and **I** is the unit tensor. By combining the perturbation theory and the normal mode expansion method [41,42], the wavefield of the generated second harmonic Lamb waves can be analytically

Table 1
The elastic constants of each ply. (Unit: GPa).

α_1	α_2	α_3	α_4	α_5	β_1	β_2
3.39	−0.78	3.74	44.79	3.06	−9.65	−15.55
β_3	β_4	β_5	β_6	β_7	β_8	β_9
−10.2	−35.7	61.45	−18.95	−10.47	163.63	42.1

* The nonlinear elastic parameters β_j are set to 0 when the material nonlinearity is excluded.

calculated. According to the perturbation theory, the nonlinear driving forces are obtained by substituting the linear wavefield quantities into the quadratic terms (the terms with β_j in Eq. (1)). Consequently, doubling the excitation amplitude will lead to a quadrupling in the amplification of the nonlinear wave amplitude. Additionally, it is noteworthy that other background nonlinearities present in the measurement system, including nonlinearities of the adhesive bonding layers and those from the instruments, can also be effectively addressed using a second-order approximation. As a result, the amplitude-dependent nonlinear responses exhibited by these materials are anticipated to behave like material nonlinearity.

Remarkably, it is expected that the amplitude of the second harmonic waves induced by delamination will be directly proportional to the amplitude of the linear waves. In contrast, that produced by material nonlinearity will exhibit a quadratic relationship with the amplitude of the linear waves.

The theoretically revealed amplitude-dependent properties of the second Lamb waves, induced by both delamination and material nonlinearity, are subsequently validated through finite element simulations. To this end, a four-ply laminate is modeled utilizing Abaqus/Explicit, as illustrated in Fig. 2(a), with dimensions measuring 250 mm × 100 mm × 2 mm. The four plies are bonded using the "tie" constraint in Abaqus, which links the nodes on the interfacing surfaces to guarantee the continuity of displacements between adjacent layers. The mesh is refined to 0.5 mm in the X and Y directions and 0.25 mm in the Z direction, ensuring over 20 elements per smallest wavelength under consideration. Solid elements (C3D8) are utilized for the plate representation. The material's mass density is 1550 kg/m^3. For excitation, a line force in the X direction is applied to both the top and bottom edges of the plate, spanning a width of 16 mm. The excitation signal comprises a five-cycle tone burst with a center frequency of 250 kHz. Simulations

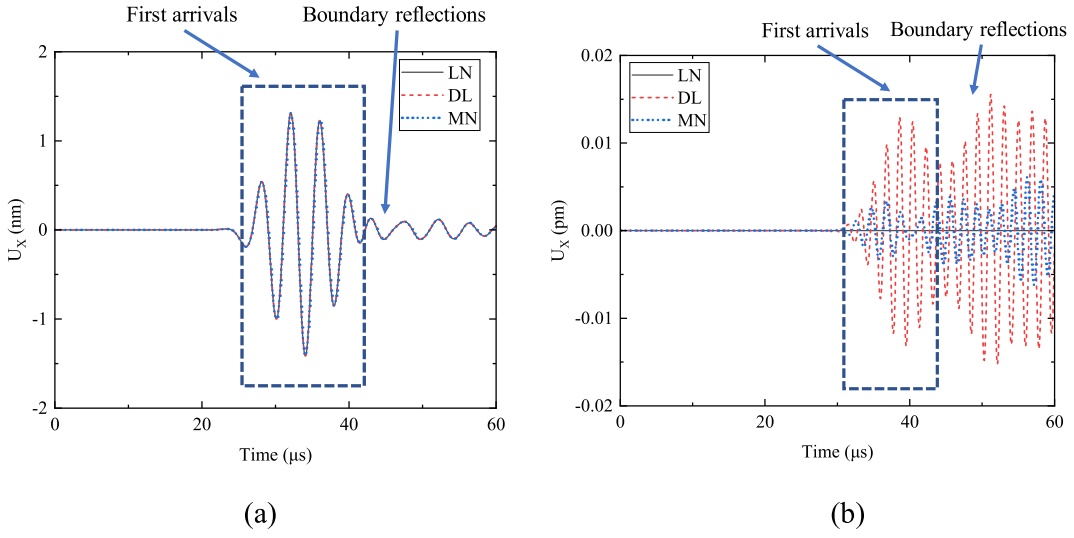

Fig. 3. (a) Linear and (b) second harmonic responses extracted at the sensing point subjecting to different types of nonlinearities (LN: linear elasticity; DL: delamination; MN: material nonlinearity).

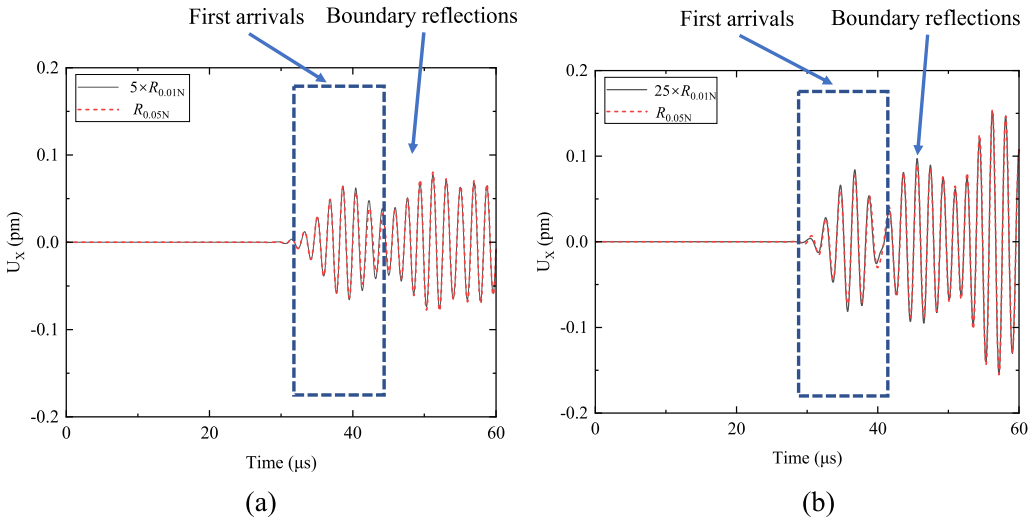

Fig. 4. Amplitude-dependent second harmonic responses in the cases of (a) delamination and (b) material nonlinearity.

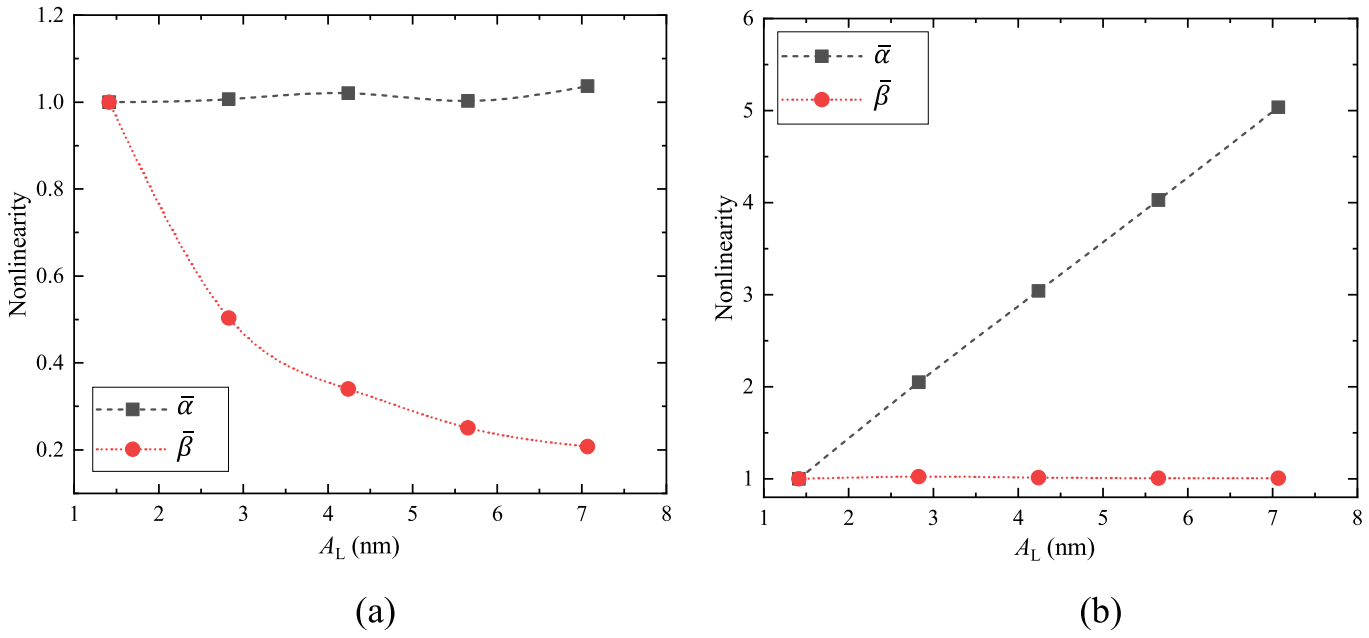

Fig. 5. Characterization of the nonlinearities from (a) delamination and (b) material nonlinearity.

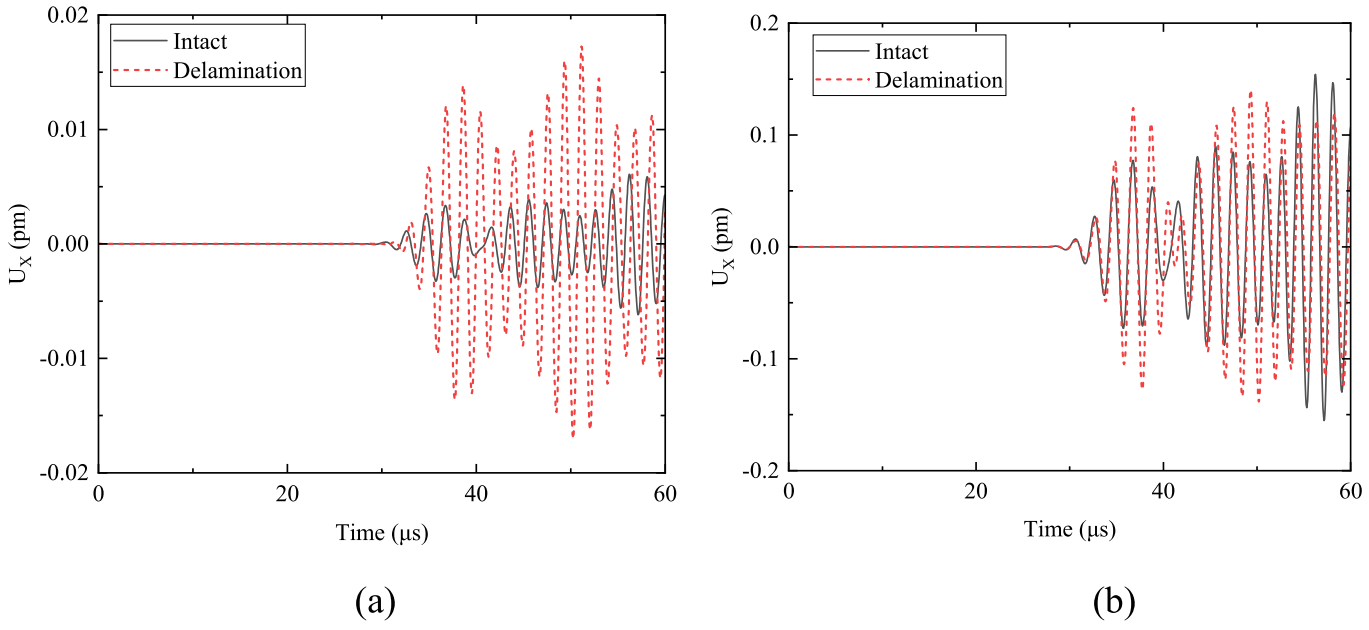

Fig. 6. Amplitude-dependent nonlinear responses before and after the introduction of delamination subjecting to the excitations of (a) 0.01 N and (b) 0.05N.

are executed with a time increment of 50 ns, corresponding to a sampling frequency of 20 MHz.

The dispersion curves of guided waves propagating at 0° in the composite plate are depicted in Fig. 2(b). As discussed in our previous research [41], the plate has no neutral plane; thus, Lamb waves are designated as B_0, B_1, B_2 … modes. According to the propagating velocities, the waves in Fig. 2(a) are identified and denoted as B_0 and B_2 waves, respectively. Initially, three separate cases are examined to verify the generation of second harmonic Lamb waves in composite plates. In the first instance, only distributed material nonlinearity (MN) is taken into account. The elastic constants for each ply are detailed in Table 1 [42]. A user material subroutine (VUMAT) is devised, incorporating Eq. (1) to represent the nonlinear elasticity of the plate. For the second case, material nonlinearity is disregarded by assigning the nonlinear elastic parameters β_j a value of 0, thus it is referred to as the linear case (LN). In the third scenario, material nonlinearity is excluded while micro delamination is introduced, measuring 1 mm × 1 mm. This delamination, between the first and second layers, is positioned 100 mm from the excitation source. During the simulations, "hard" contact is employed to mimic the "breathing" phenomenon for normal behavior. When surfaces are in contact, contact pressure can be transmitted between them. Surfaces will separate if the contact pressure decreases to zero. Separated surfaces come back into contact again when the gap between them reduces to zero. Regarding tangential behavior, a frictionless formulation is adopted for the contact surfaces. In all three calculation scenarios, the amplitude of the applied forces is set to 0.01 N. The displacement in the *X* direction at the sensing point (U_X) is monitored as the system response.

The linear responses in the three cases are shown in Fig. 3(a). The

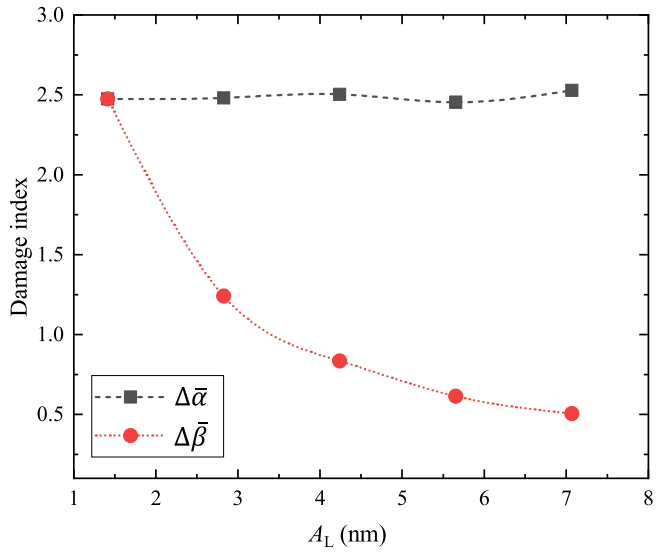

Fig. 7. Extracted damage indices before and after the introduction of delamination.

first arrivals in the signals correspond to the B_2 mode Lamb waves [41], which have the highest velocity and are therefore advantageous for signal analyses in SHM applications. It is evident that both material nonlinearity and delamination have a negligible effect on the linear Lamb waves. The second harmonic responses are subsequently extracted using the phase-inverse method [39]. This involves applying a pair of excitation signals with inverted phases and then superimposing their corresponding responses to extract the nonlinear responses. In principle, the extracted nonlinear responses should consist of all even-order harmonic waves and a static component. In the simulations, a tone-burst excitation signal was chosen with a central frequency of 250 kHz, which resulted in second harmonic waves at 500 kHz. Consequently, a Butterworth filter with a passband ranging from 375 kHz to 625 kHz is utilized to isolate the second harmonic component. The resulting second harmonic responses in the three cases are shown in Fig. 3(b). It is observed that both delamination and material nonlinearity lead to the generation of second harmonic Lamb waves. Despite the composite plate's limited size, which results in boundary reflections from the edges being present in the nonlinear responses, the first arrivals can still be distinguished and extracted for further analysis.

Subsequently, the amplitude-dependent characteristics of the second harmonic Lamb waves are examined. Five sets of simulations are performed with the amplitude of the applied forces varying from 0.01 N to 0.05 N, in increments of 0.01 N. Fig. 4 displays the typical second harmonic responses resulting from delamination and material nonlinearity under excitations of 0.01 N and 0.05 N, denoted as $R_{0.01N}$ and $R_{0.05N}$, respectively. Specifically, the $R_{0.01N}$ response induced by the delamination is amplified by a factor of 5 and compared with $R_{0.05N}$ in Fig. 4(a), revealing a satisfactory agreement between them. Conversely, the $R_{0.01N}$ response induced by material nonlinearity requires amplification by a factor of 25 to align with $R_{0.05N}$ in Fig. 4(b).

In order to more accurately quantify the amplitude-dependent features, two parameters, α' and β', are defined to characterize the nonlinearities as follows

$$\alpha' = \frac{A_2}{A_1} \tag{2a}$$

$$\beta' = \frac{A_2}{{A_1}^2} \tag{2b}$$

where A_1 and A_2 represent the amplitudes of the linear and second harmonic waves, respectively. Specifically, the linear and second harmonic time-domain signals are processed with complex Morlet wavelet transform. Subsequently, the amplitudes are extracted as the first peak in the wavelet coefficients [43].

The rationale behind defining the parameters is that their values should not change with the wave excitation amplitudes for a given damage or nonlinear source. Otherwise, characterizing damage would become a challenging task. More specifically, as discussed above, when considering the "breathing" effect related to delamination, one might expect that if the amplitude of the incident waves is doubled, the received time domain response should also be doubled, thus justifying the use of the parameter α' to characterize delamination. Material nonlinearity can be described as quadratic nonlinearity. If the excitation amplitude is doubled, there will be a consequential fourfold increase in the amplification of the nonlinear wave amplitude. Consequently, the

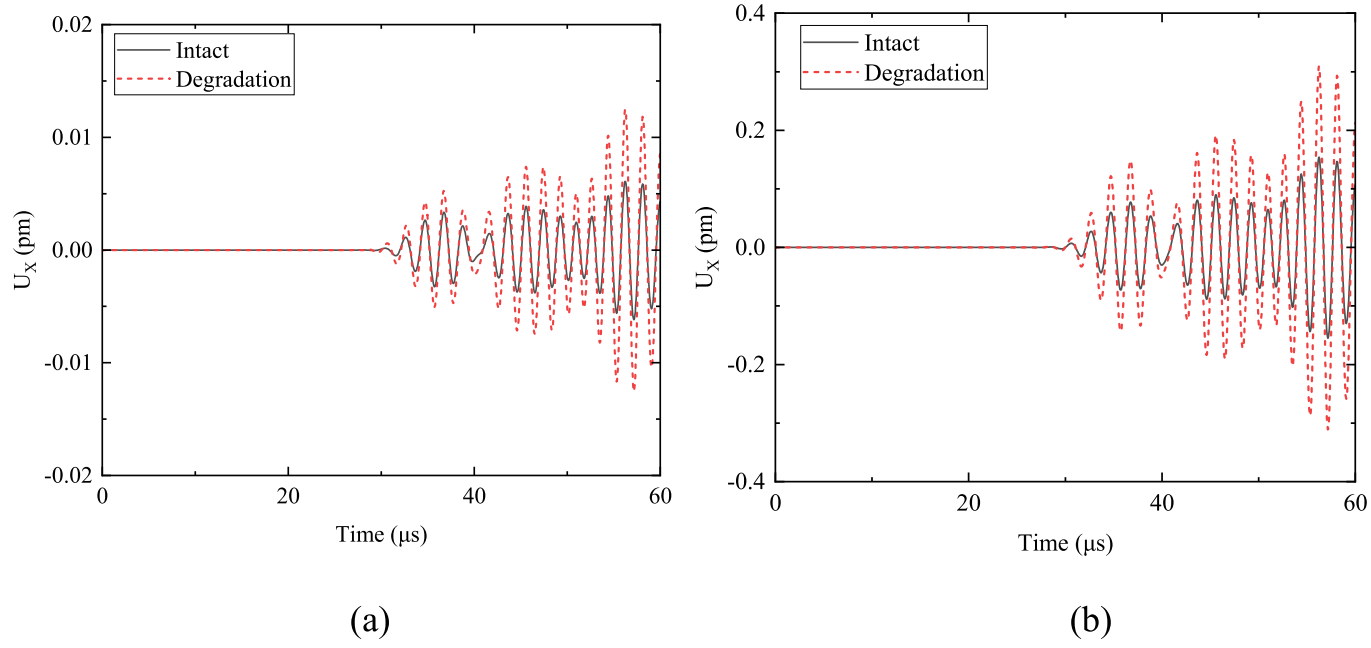

Fig. 8. Amplitude-dependent nonlinear responses before and after the introduction of material degradation subjecting to the excitations of (a) 0.01 N and (b) 0.05N.

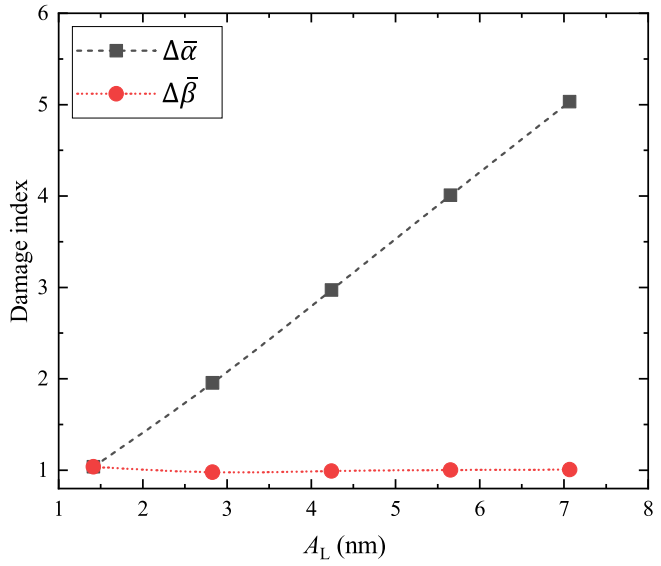

Fig. 9. Extracted damage indices before and after the introduction of material degradation.

parameter β' is defined to characterize material nonlinearity. Therefore, the use of α' and β' can effectively characterize and discriminate delamination and material nonlinearity.

Following the calculation of the α' and β', in the five cases with varying excitation levels, a normalization process was conducted with respect to the parameters in the 0.01-N case (α'_0 and β'_0). The normalized α' and β' are denoted as $\bar{\alpha}$ and $\bar{\beta}$ respectively as:

$$\bar{\alpha} = \frac{\alpha'}{\alpha'_0} \tag{3a}$$

$$\bar{\beta} = \frac{\beta'}{\beta'_0} \tag{3b}$$

Consequently, the resulting values of $\bar{\alpha}$ and $\bar{\beta}$ associated with delamination and material nonlinearity are determined for various excitation levels, as depicted in Fig. 5. The amplitude of the first arrival in the linear response (A_L) is utilized as the horizontal axis, which is extracted using the Hilbert transform. It is apparent that the two types of nonlinearities display distinct amplitude-dependent characteristics. Specifically, the parameter $\bar{\alpha}$ remains largely unchanged in the case of delamination, while $\bar{\beta}$ remains stable in the case of material nonlinearity, in agreement with theoretical analyses. Additionally, it is noteworthy that other combinations of contact behaviors have been examined, including a "Softened" contact model, defined by a linear function for normal behavior, and a "Rough" (no-slip) model and a basic Coulomb friction model for tangential behavior. The absolute values of the resultant second harmonic Lamb waves may be slightly influenced by different contact models, yet the fundamental trends of the amplitude-dependent second-harmonic waves persist.

3. A delamination discrimination strategy

The acquired knowledge on the amplitude-dependent second Lamb waves allows for conceiving a damage identification strategy that is capable of discriminating delamination from background nonlinearities, exemplified by material nonlinearity. Within the realm of SHM, a benchmark baseline is recorded as a reference. Subsequent tests are performed on a continuous basis, wherein the elicited responses are juxtaposed with the baseline signal. Taking into account the distinct amplitude-dependent traits of the second Lamb waves, two specific damage indices are defined to enhance the precision and reliability of damage detection in composite structures.

$$\Delta\bar{\alpha} = \frac{\mathrm{Peak}\left(\left|W_t^{2f}(t) - W_b^{2f}(t)\right|\right)}{A_{1b}\alpha'_0} \tag{4a}$$

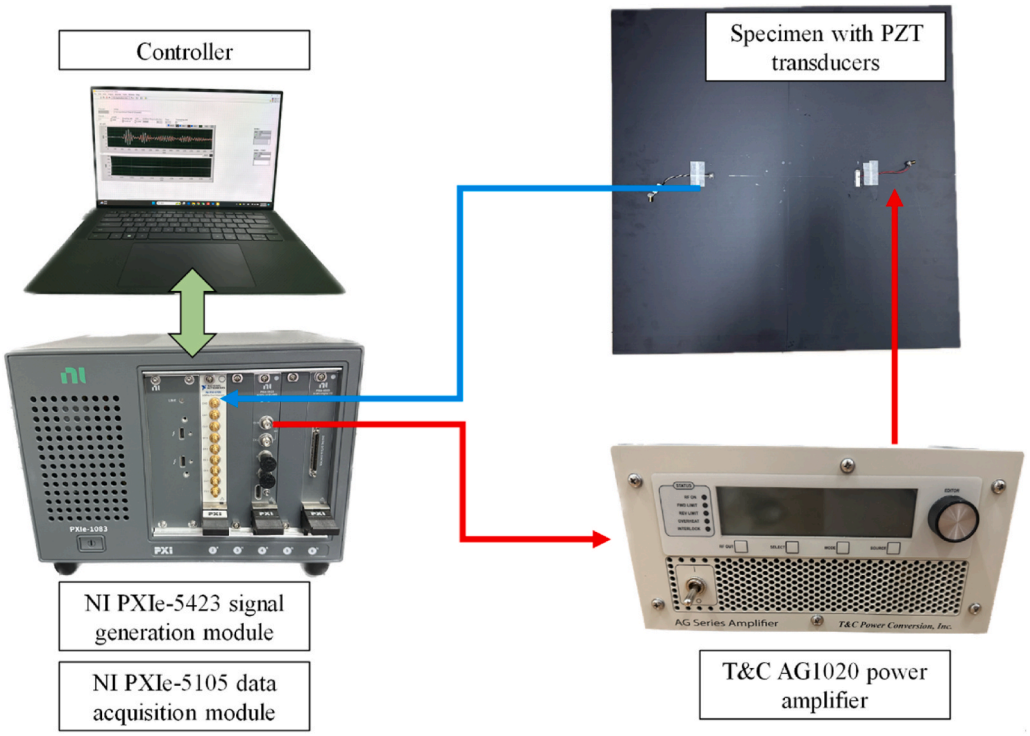

Fig. 10. Experimental setup.

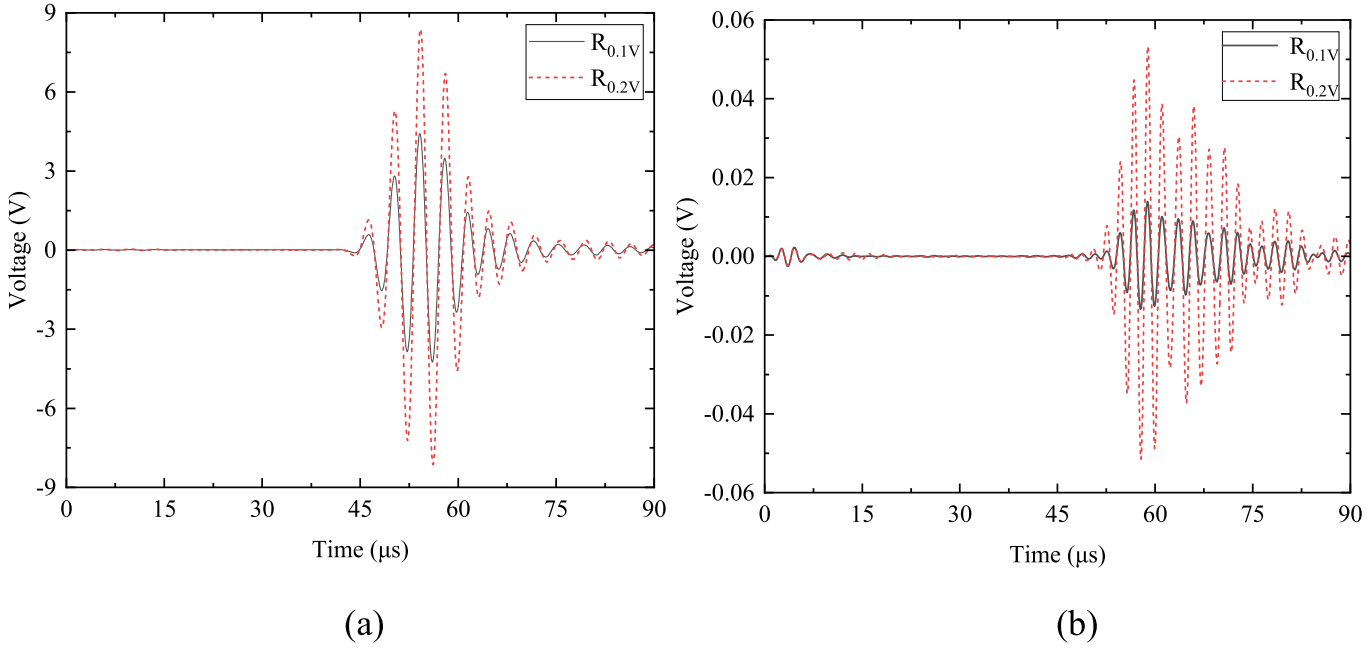

Fig. 11. Amplitude-dependent (a)linear and (b)nonlinear responses subjecting to the input excitation amplitude of (a) 0.1 V and (b) 0.2 V.

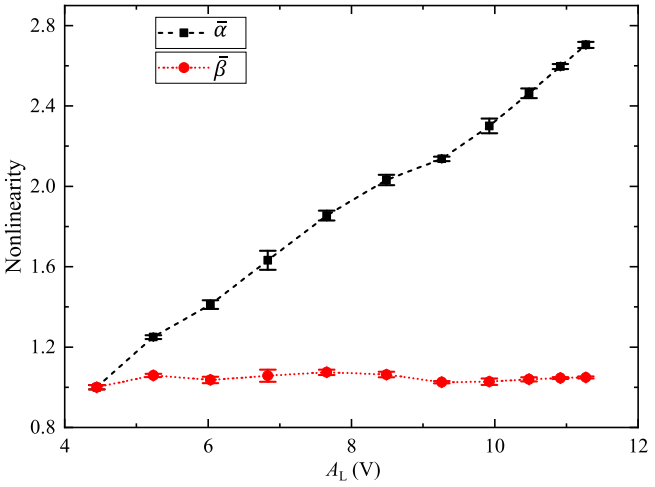

Fig. 12. Characterization of the nonlinearities of the system.

$$\Delta\bar{\beta} = \frac{\mathrm{Peak}\left(\left|W_t^{2f}(t) - W_b^{2f}(t)\right|\right)}{{A_{1b}}^2\beta_0'} \tag{4b}$$

The subscripts t and b in the above definitions are associated with the test and baseline signals, respectively. $W^{2f}(t)$ denotes the absolute values of the wavelet coefficients extracted at the second harmonic frequency [43]. The function Peak is used to extract the peak value of the first arrival. In physical terms, the two damage indices quantify the relative change in the nonlinearities contained in α' and β'. Consequently, it can be postulated that delamination is more likely to occur when $\Delta\bar{\alpha}$ approaches a constant. In contrast, alterations in the background nonlinearity will result in a more stable and flatter $\Delta\bar{\beta}$.

Subsequently, finite element simulations are conducted to validate the proposed strategy. As a baseline, a scenario involving an intact structure with material nonlinearity is simulated. First, the delamination is introduced. The dimensions and contact properties of the additional delamination are consistent with those described in the previous section. The nonlinear responses elicited by excitations of 0.01 N and 0.05 N are depicted in Fig. 6(a) and (b), respectively. The inclusion of the delamination leads to an amplification of the second harmonic responses, which exhibit distinct amplitude-dependent characteristics. Thereafter, the damage indices are computed and plotted in Fig. 7. It is evident that the value of the damage index $\Delta\bar{\alpha}$ remains nearly constant, indicating the presence of delamination.

The ensuing examination of material degradation involves a deliberate doubling of the nonlinear elastic constants β_j. Such modifications in β_j can be attributed to a plethora of real-world influences, encompassing distributed fatigue and thermal aging. It is crucial to underscore that the simulated degradation herein serves as a paradigmatic illustration, aimed at elucidating the effects of underlying nonlinearities on damage diagnostics. In alignment with the methodology delineated earlier, the characteristic second harmonic responses elicited by excitations of 0.01 N and 0.05 N are respectively depicted in Fig. 8(a) and (b). As postulated, an augmentation in the values of β_j corresponds directly to a proportional increase in the magnitude of the second harmonic response, irrespective of the applied excitation amplitude. The quantification of damage, as represented by the damage indices, is articulated in Fig. 9. Notably, in this scenario, the designated parameter $\Delta\bar{\beta}$ basically keeps constant across the entire variation range of the linear wave amplitudes, indicating a variation of material nonlinearity. To conclude, the simulations firmly underscore the robustness of the proposed method for discerning delamination.

4. Experimental validations

Experiments are conducted to verify the theoretically and numerically predicted amplitude-dependent characteristics of the second Lamb waves and to evaluate the effectiveness of the proposed delamination detection strategy. A 10-ply carbon fiber-reinforced plate (CFRP) with dimensions of 600 mm × 600 mm × 2 mm and a stack of $[0°/90°]_5$ is tested as shown in Fig. 10, in conjunction with the requisite measurement apparatus. Two piezoelectric transducers (PZT) are bonded to the plate using a two-component epoxy adhesive (UHU®). The actuator has dimensions of 30 mm × 8 mm × 0.5 mm, while the sensor measures 5 mm × 5 mm × 0.5 mm, with a separation distance of 260 mm between them. The excitation signal consisted of a 5-cycle tone burst at 250 kHz. It is worth noting that the reported amplitude-dependent features of the

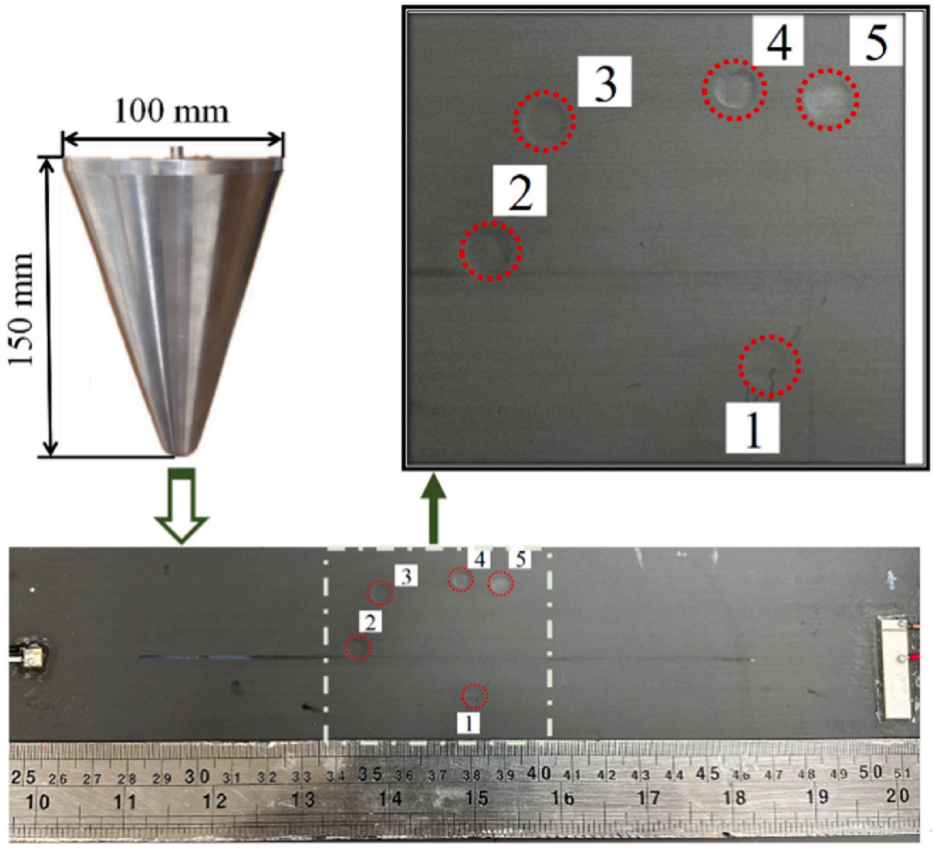

Fig. 13. Scheme of the impact testing.

second harmonic Lamb waves should not be influenced by the frequency of the fundamental waves according to theoretical analyses. Thus, in principle, other frequencies could also be utilized. However, in experimental settings, since PZT actuators are employed, the frequency can impact the amplitude of the excited waves. Specifically, an 8 mm-wide PZT is used in this case. Through sweeping the excitation frequencies, it is observed that the amplitude of the generated B_2 mode waves at 250 kHz is relatively large, which facilitates measurement. To maintain consistency, this frequency is adopted in the simulations.

The system operates as follows: a National Instruments® (NI) PXIe-5423 signal generator outputs the designated tone burst signal to the T&C® AG1020 power amplifier, whose output is configured to 3W to drive PZT actuators for wave generation. Subsequently, the piezoelectric transducers (PZT) sensors capture the excited Lamb waves, which are recorded with a National Instruments PXIe-5105 data acquisition module. As previously stated, the phase-inverse approach is utilized to extract the nonlinear responses. The amplitudes of the excitation signals range from 0.1 V to 0.3 V, with an interval of 0.02 V. To quantify the measurement uncertainty, four trials are conducted for each setting. Each trial involves taking an average of 100 measurements to reduce the influence of random noise. In the experiments, ultrasonic tests were conducted four times, and the error bars represent the standard deviation of the target parameters across these tests, thereby revealing the uncertainty in the measurement.

Firstly, the nonlinear properties of the entire system are analyzed. Typical linear and nonlinear responses corresponding to 0.1 V and 0.2 V excitations are presented in Fig. 11(a) and (b), respectively. It can be observed that the doubling of the excitation level also roughly doubles the linear response, while the second harmonic response is amplified by a factor of approximately four. To provide a more detailed illustration of this phenomenon, the amplitudes of the waves are presented with respect to the linear wave amplitudes, as shown in Fig. 12. It can be observed that the coefficient of quadratic nonlinearity $\overline{\beta}$ remains almost constant, indicating that the quadratic nonlinearity induced by background nonlinearities is dominant in the system. This is consistent with our expectations, given that the plate is in its original and unmodified state.

Subsequently, the dropping weight technique is employed to introduce impact damage into the plate, as shown in Fig. 13. As documented in the literature, impact can effectively induce delamination in composite plates [38]. In this instance, the impact energy is approximately 3 J. The impact is applied five times, resulting in the formation of five distinct pits as illustrated in Fig. 13. After each impact, measurements are conducted to investigate the impact damage's effect on the nonlinear waves.

In principle, delamination can generate not only second harmonic waves but also higher-order harmonics. To determine the dominance level of different harmonics, a representative measured signal after three impacts subject to a 0.3-V excitation is presented in Fig. 14(a). The corresponding spectrum is calculated as shown in Fig. 14(b). It can be observed that although the third and higher-order harmonics are discernible, their intensities are significantly lower than the second harmonic. As a result, we concentrate on the second harmonic due to its prominence.

The influence of delamination on guided waves is then evaluated. As a representative case, the linear and second harmonic responses subject to a 0.1-V excitation before impact and after three impacts are presented in Fig. 15(a) and (b), respectively. While the linear Lamb waves remain largely unaffected by the impact damage, a significant increase in the amplitude of the second harmonic waves is observed, demonstrating the increased sensitivity of the nonlinear waves to the impact-induced delamination.

In order to ascertain the characteristics of the damage-induced second harmonic Lamb waves, the damage indices $\Delta\overline{\alpha}$ and $\Delta\overline{\beta}$ are calculated

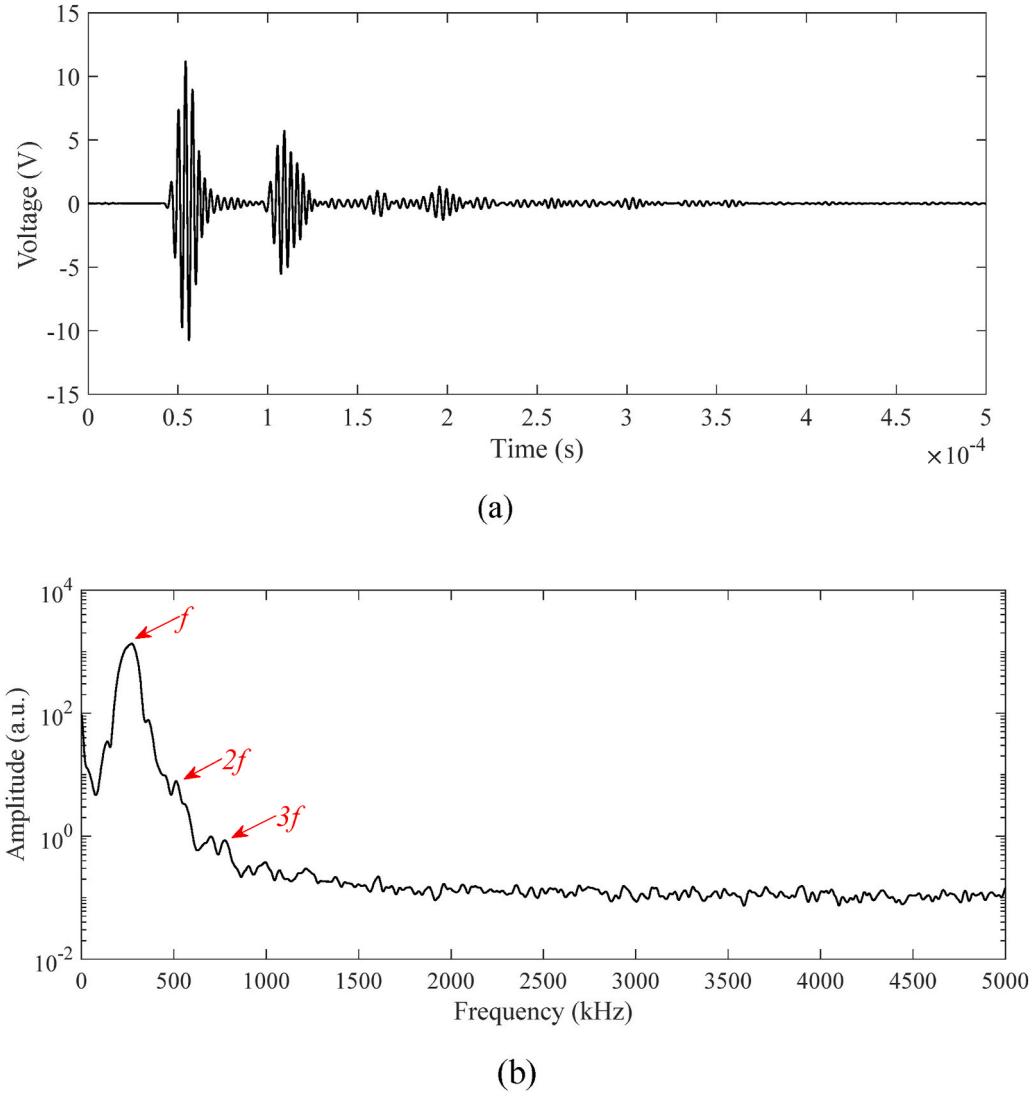

Fig. 14. (a) Typical time-domain response and (b) its spectrum after the introduction of three impacts subjecting to the input excitation amplitude of 0.3 V.

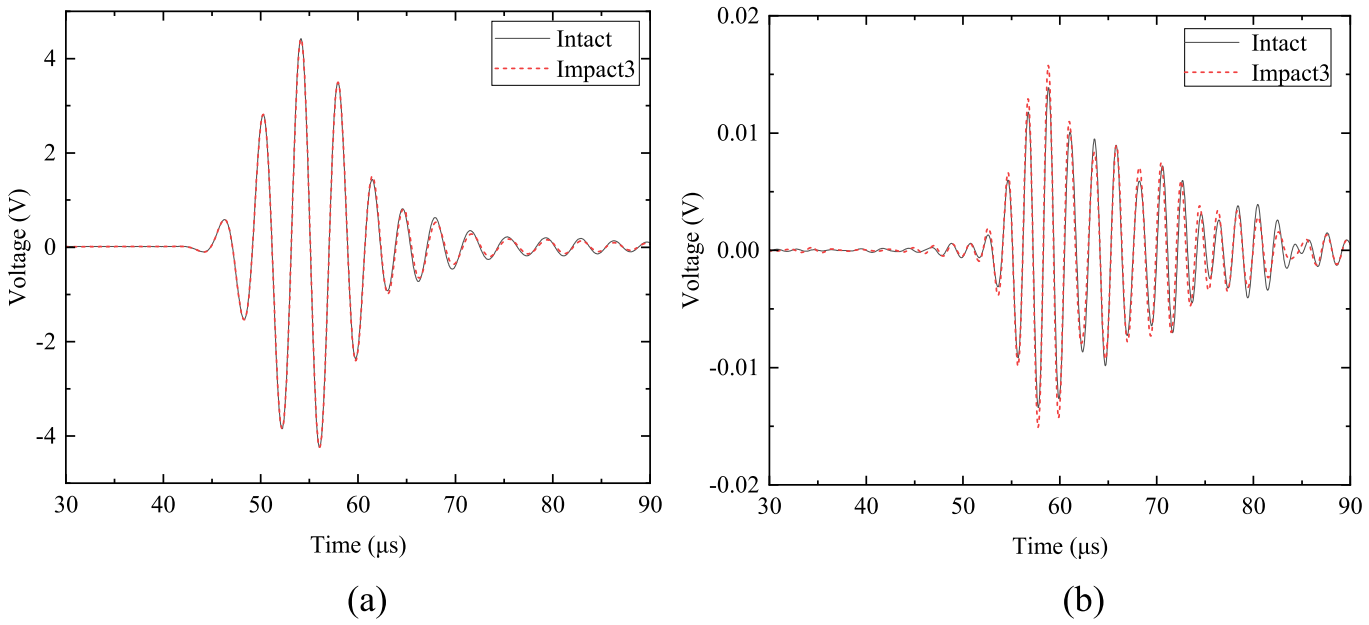

Fig. 15. Typical (a) linear and (b) nonlinear responses before and after the introduction of three impacts subjecting to the input excitation amplitude of 0.1 V.

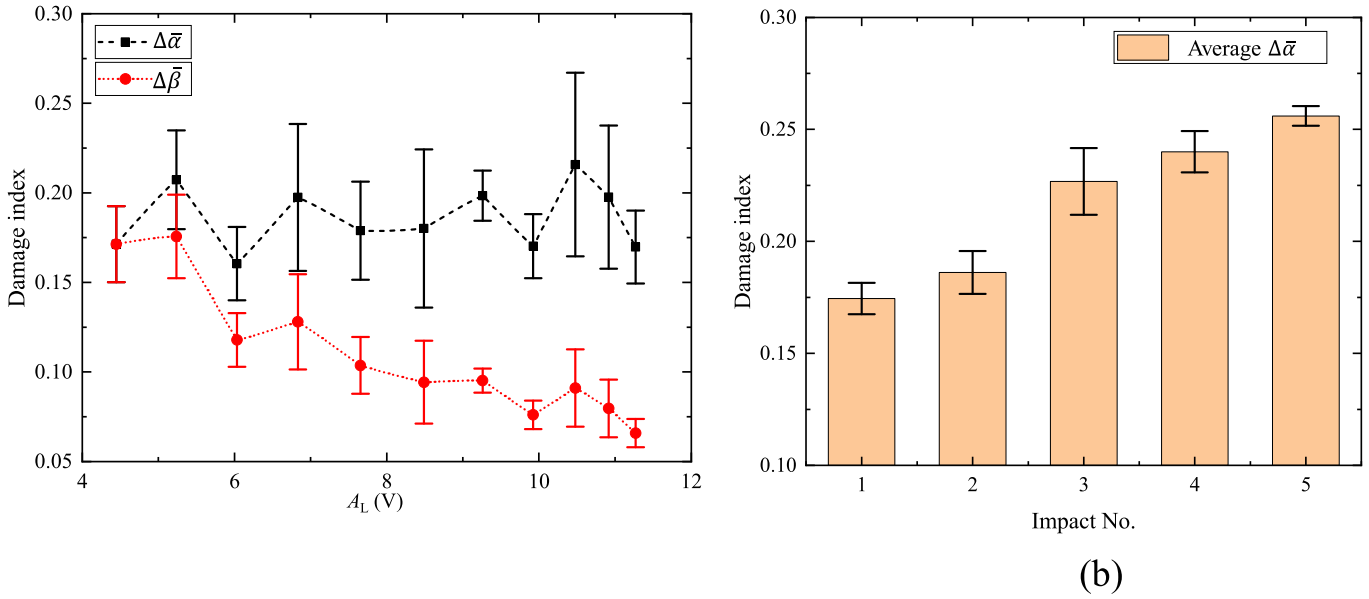

Fig. 16. (a) Damage indices before and after the introduction of three impacts; (b) the extracted damage indices for different impacts.

in accordance with the methodology illustrated in Fig. 16(a). It can be observed that the $\Delta\bar{\alpha}$ is more stable with respect to the excitation voltage, whereas the $\Delta\bar{\beta}$ exhibits greater variation. This suggests that the induced impact damage is more likely to manifest as delamination. Subsequently, the averaged values of $\Delta\bar{\alpha}$ with respect to the linear wave amplitudes are extracted in order to quantify the damage severity for each impact case, with results shown in Fig. 16(b). A monotonic increase in the averaged $\Delta\bar{\alpha}$ is observed with the increase in the number of impacts. This trend illustrates the effectiveness of the proposed method for the quantification of delamination in future applications.

Finally, the influences of the variations in background nonlinearities on SHM are evaluated through a dedicated heating process, which is designed to effectively alter the material nonlinearity [41]. In particular, a platform measuring 100 mm × 100 mm is employed to heat the center of the plate to a maximum temperature of 112.4 °C, as illustrated in Fig. 17. Measurements are taken before and after the heating process, with the typical linear and second harmonic responses shown in Fig. 18 (a) and (b), respectively. Apart from the slight changes in the signal phase, the linear wave amplitude remains almost unchanged, whereas the second harmonic amplitude is increased after the heating is applied. This suggests that thermal effects exercise a more significant influence on the nonlinear waves than on the linear waves.

The same procedure is followed to calculate the $\Delta\bar{\alpha}$ and $\Delta\bar{\beta}$, with the results shown in Fig. 19. It can be observed that $\Delta\bar{\beta}$ is basically constant with respect to the linear wave amplitude. This suggests that the heating primarily affects the background nonlinearities rather than introducing new delamination. By synthesizing the results presented in Fig. 16(a) and 19, it can be concluded that the proposed method offers an effective means to discern between delamination and background nonlinearities in composite plates. It is worth noting we did not implement any specific techniques to reduce background nonlinearities. Even in the presence of strong background nonlinearities, the proposed method still allows to

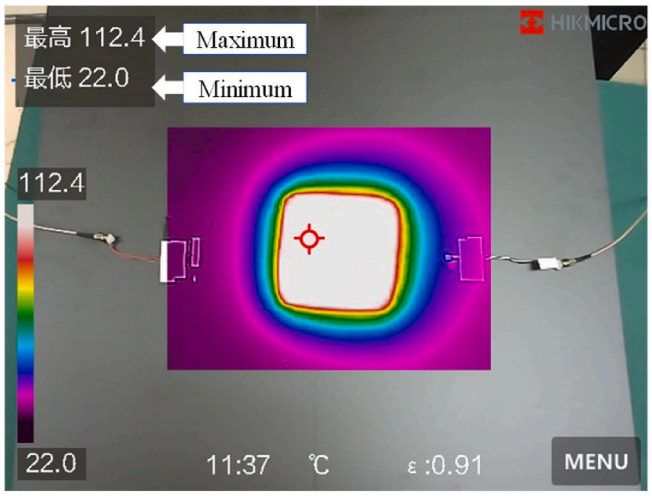

Fig. 17. Scheme of the heating process.

discern the nonlinearity induced by delamination in typical SHM applications. This ability to differentiate damage types and background material effects is crucial and might be an asset for SHM applications.

Remarkably, in practical scenarios, there are two distinct cases necessitating the differentiation between delamination and material nonlinearity. The first case pertains to SHM. During continuous monitoring of the variation of the second harmonic waves in a structure, it is necessary to determine whether these changes are caused by delamination or material nonlinearity. This is readily achieved by the proposed method, as substantiated by both simulations and experiments. The second scenario falls within the realm of non-destructive evaluation (NDE). For a given structure embedding both delamination and material nonlinearity, there is a need to distinguish the second harmonic Lamb waves induced by each. Nonetheless, owing to their respective and distinct generation mechanisms and characteristics, namely material nonlinearity typically originates from a distributed source and delamination from a localized one, the interaction of these two types of second harmonic Lamb waves becomes intricate. Although the reported amplitude-dependent attributes might provide alternative means to differentiate these wave types, a comprehensive examination and meticulously developed algorithms are essential to address this challenge. This study mainly focuses on SHM applications, while NDE applications will be explored in future research.

5. Conclusions

The amplitude-dependent characteristics of the second harmonic Lamb waves, induced by delamination and material nonlinearity in composite structures, are examined to discern their influences on SHM applications. Based on the observed features, a novel strategy is proposed to differentiate the second harmonic Lamb wave components generated by delamination and those originating from background nonlinearities exemplified by the inherent material nonlinearity in composites. Prior to implementing this strategy, finite element validations are conducted to confirm the amplitude-dependent features of the second harmonic Lamb waves and to assess the effectiveness of the proposed approach. To further demonstrate the efficacy of the proposed method for delamination detection, additional experiments are con-

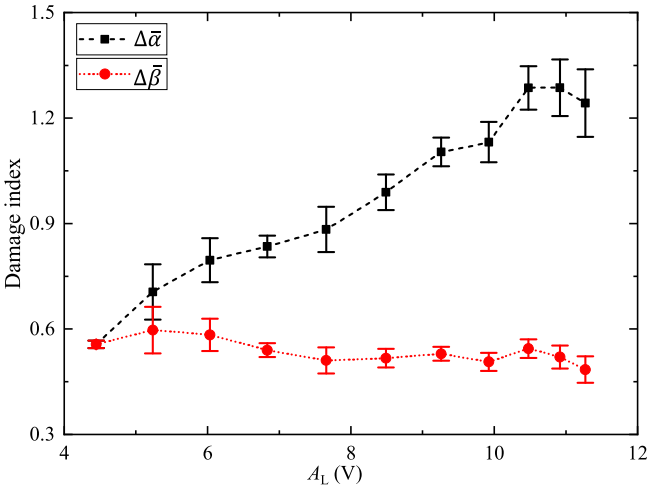

Fig. 19. Extracted damage indices before and after the heating process.

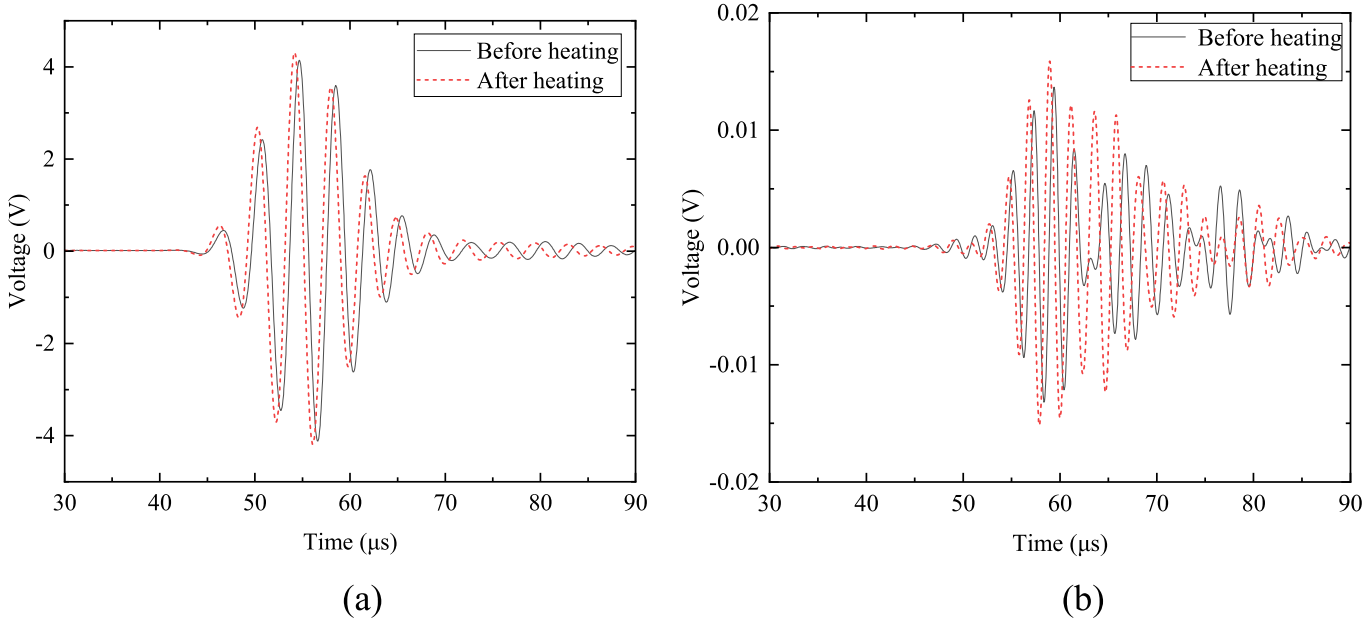

Fig. 18. Typical (a) linear and (b) nonlinear responses before and after the heating process subjecting to the input excitation amplitude of 0.1 V.

ducted, considering both impact-induced delamination and heat-induced changes in material properties.

It is shown that the amplitude of the delamination-induced second harmonic waves is linearly proportional to the fundamental wave amplitude, whereas that from material nonlinearity exhibits a quadratic relationship with the fundamental wave amplitude. Consequently, two damage indices are proposed and proved to be an effective means to discriminate the two types of nonlinear sources.

The results illuminate the mechanisms of the second harmonic generation from diverse nonlinear sources, paving the way for practical delamination detection in composite structures. Furthermore, as the proposed delamination detection method only requires varying excitation levels without complicating the physical measurement system, it showcases significant potential for engineering applications. In a broader context, this research also supplements the current guided wave theory from an amplitude-dependent perspective, laying the groundwork for further exploration into various nonlinear guided wave phenomena.

CRediT authorship contribution statement

Shengbo Shan: Writing – original draft, Methodology, Investigation, Funding acquisition, Conceptualization. **Chi Zhang:** Writing – review & editing, Validation, Methodology, Investigation. **Gujun Wu:** Writing – review & editing, Validation, Investigation. **Yang Song:** Validation, Methodology, Investigation. **Ze Liu:** Validation, Investigation. **Yuanman Zhang:** Validation, Investigation. **Li Cheng:** Writing – review & editing, Supervision, Resources, Funding acquisition.

Declaration of competing interest

The authors declare that they have no known competing financial interests or personal relationships that could have appeared to influence the work reported in this paper.

Data availability

Data will be made available on request.

Acknowledgments

The research was funded by grants from the National Natural Science Foundation of China (12302114), the Research Grants Council of Hong Kong Special Administrative Region (PolyU 152013/21E), the Natural Science Foundation of Shanghai (22ZR1462700), the Fundamental Research Funds for the Central Universities, Shanghai Gaofeng Project for University Academic Program Development, and the Innovation and Technology Commission of the HKSAR Government to the Hong Kong Branch of National Rail Transit Electrification and Automation Engineering Technology Research Center (K-BBY1).

References

[1] Sharma H, Kumar A, Rana S, Sahoo NG, Jamil M, Kumar R, Sharma S, Li C, Kumar A, Eldin SM. Critical review on advancements on the fiber-reinforced composites: role of fiber/matrix modification on the performance of the fibrous composites. J Mater Res Technol 2023;26:2975–3002.
[2] Ranjbar N, Zhang M. Fiber-reinforced geopolymer composites: a review. Cement Concr Compos 2020;107:103498.
[3] Alnuaimi H, Amjad U, Park S, Russo P, Lopresto V, Kundu T. An improved nonlinear ultrasonic technique for detecting and monitoring impact induced damage in composite plates. Ultrasonics 2022;119:106620.
[4] Falcó O, Lopes C, Sommer D, Thomson D, Ávila R, Tijs B. Experimental analysis and simulation of low-velocity impact damage of composite laminates. Compos Struct 2022;287:115278.
[5] De Luca A, Caputo F, Khodaei ZS, Aliabadi M. Damage characterization of composite plates under low velocity impact using ultrasonic guided waves. Compos B Eng 2018;138:168–80.
[6] Zhang H, Sun J, Rui X, Liu S. Delamination damage imaging method of CFRP composite laminate plates based on the sensitive guided wave mode. Compos Struct 2023;306:116571.
[7] Memmolo V, Monaco E, Boffa N, Maio L, Ricci F. Guided wave propagation and scattering for structural health monitoring of stiffened composites. Compos Struct 2018;184:568–80.
[8] Ricci F, Monaco E, Boffa ND, Maio L, Memmolo V. Guided waves for structural health monitoring in composites: a review and implementation strategies. Prog Aero Sci 2022;129:100790.
[9] Gharehbaghi VR, Noroozinejad Farsangi E, Noori M, Yang T, Li S, Nguyen A, Málaga-Chuquitaype C, Gardoni P, Mirjalili S. A critical review on structural health monitoring: definitions, methods, and perspectives. Archives of computational methods in engineering; 2021. p. 1–27.
[10] Cawley P. Structural health monitoring: closing the gap between research and industrial deployment. Struct Health Monit 2018;17:1225–44.
[11] Mitra M, Gopalakrishnan S. Guided wave based structural health monitoring: a review. Smart Mater Struct 2016;25:053001.
[12] Shen Y, Cesnik CE. Local interaction simulation approach for efficient modeling of linear and nonlinear ultrasonic guided wave active sensing of complex structures. J Nondestructive Evaluation, Diagnostics Prognostics Eng Sys 2018;1. 011008-011008-011009.
[13] Yang Z, Yang H, Tian T, Deng D, Hu M, Ma J, Gao D, Zhang J, Ma S, Yang L. A review in guided-ultrasonic-wave-based structural health monitoring: from fundamental theory to machine learning techniques. Ultrasonics 2023:107014.
[14] Bjørheim F, Siriwardane SC, Pavlou D. A review of fatigue damage detection and measurement techniques. Int J Fatig 2022;154:106556.
[15] Kaewniam P, Cao M, Alkayem NF, Li D, Manoach E. Recent advances in damage detection of wind turbine blades: a state-of-the-art review. Renew Sustain Energy Rev 2022;167:112723.
[16] Lissenden CJ. Nonlinear ultrasonic guided waves—principles for nondestructive evaluation. J Appl Phys 2021;129.
[17] Chillara VK, Lissenden CJ. Review of nonlinear ultrasonic guided wave nondestructive evaluation: theory, numerics, and experiments. Opt Eng 2016;55:011002. 011002.
[18] Zhao G, Jiang M, Luo Y, Sui Q. Third harmonic approximate phase velocity matching nonlinear early fatigue damage detection. Measurement 2022;189:110518.
[19] Hasanian M, Lissenden CJ. Second order harmonic guided wave mutual interactions in plate: vector analysis, numerical simulation, and experimental results. J Appl Phys 2017;122.
[20] Jiang C, Zhang C, Li W, Deng M, Ng C-T. Assessment of damage in composites using static component generation of ultrasonic guided waves. Smart Mater Struct 2022;31:045025.
[21] Allen JCP, Ng CT. Debonding detection at adhesive joints using nonlinear Lamb waves mixing. NDT E Int 2022;125:102552.
[22] Zhu W, Xu Z, Xiang Y, Liu C, Deng M, Qiu X, Sun D, Xuan F. Nonlinear ultrasonic detection of partially closed cracks in metal plates using static component of lamb waves. NDT E Int 2021;124:102538.
[23] Cho H, Hasanian M, Shan S, Lissenden CJ. Nonlinear guided wave technique for localized damage detection in plates with surface-bonded sensors to receive Lamb waves generated by shear-horizontal wave mixing. NDT E Int 2019;102:35–46.
[24] Allen JCP, Ng CT. Damage detection in composite laminates using nonlinear guided wave mixing. Compos Struct 2023;311:116805.
[25] Soleimanpour R, Ng C-T. Scattering analysis of nonlinear Lamb waves at delaminations in composite laminates. J Vib Control 2022;28:1311–23.
[26] Sikdar S, Ostachowicz W, Kundu A. Deep learning for automatic assessment of breathing-debonds in stiffened composite panels using non-linear guided wave signals. Compos Struct 2023;312:116876.
[27] Wei L, Chen J. Characterization of delamination features of orthotropic CFRP laminates using higher harmonic generation technique: experimental and numerical studies. Compos Struct 2022;285:115239.
[28] Yelve NP, Mitra M, Mujumdar P. Detection of delamination in composite laminates using Lamb wave based nonlinear method. Compos Struct 2017;159:257–66.
[29] Yelve NP, Mitra M, Mujumdar P, Ramadas C. A hybrid method based upon nonlinear Lamb wave response for locating a delamination in composite laminates. Ultrasonics 2016;70:12–7.
[30] Chronopoulos D. Calculation of guided wave interaction with nonlinearities and generation of harmonics in composite structures through a wave finite element method. Compos Struct 2018;186:375–84.
[31] Apalowo R, Chronopoulos D, Cantero-Chinchilla S. Wave interaction with nonlinear damage and generation of harmonics in composite structures. Compos Struct 2019;230:111495.
[32] Solodov IY, Krohn N, Busse G. CAN: an example of nonclassical acoustic nonlinearity in solids. Ultrasonics 2002;40:621–5.
[33] Kim Y, Choi S, Jhang K-Y, Kim T. Experimental verification of contact acoustic nonlinearity at rough contact interfaces. Materials 2021;14:2988.
[34] Delrue S, Van Den Abeele K. Detection of defect parameters using nonlinear air-coupled emission by ultrasonic guided waves at contact acoustic nonlinearities. Ultrasonics 2015;63:147–54.
[35] Wang K, Liu M, Su Z, Yuan S, Fan Z. Analytical insight into "breathing" crack-induced acoustic nonlinearity with an application to quantitative evaluation of contact cracks. Ultrasonics 2018;88:157–67.
[36] Broda D, Staszewski WJ, Martowicz A, Uhl T, Silberschmidt V. Modelling of nonlinear crack–wave interactions for damage detection based on ultrasound—a review. J Sound Vib 2014;333:1097–118.

[37] Rauter N, Lammering R. Impact damage detection in composite structures considering nonlinear lamb wave propagation. Mech Adv Mater Struct 2015;22:44–51.
[38] Tie Y, Zhang Q, Hou Y, Li C. Impact damage assessment in orthotropic CFRP laminates using nonlinear Lamb wave: experimental and numerical investigations. Compos Struct 2020;236:111869.
[39] Shan S, Cheng L, Li P. Adhesive nonlinearity in Lamb-wave-based structural health monitoring systems. Smart Mater Struct 2016;26:025019.
[40] Shan S, Wen F, Cheng L. Purified nonlinear guided waves through a metamaterial filter for inspection of material microstructural changes. Smart Mater Struct 2021;30:095017.
[41] Shan S, Ke R, Ma Y, Song Y, Cheng L. Quasi-phase-matched nonlinear Lamb waves in composite laminates for material degradation monitoring. NDT E Int 2024;143:103064.
[42] Zhao J, Chillara VK, Ren B, Cho H, Qiu J, Lissenden CJ. Second harmonic generation in composites: theoretical and numerical analyses. J Appl Phys 2016;119.
[43] Shan S, Qiu J, Zhang C, Ji H, Cheng L. Multi-damage localization on large complex structures through an extended delay-and-sum based method. Struct Health Monit 2016;15:50–64.